J. Coat. Technol. Res., **18** (3) 665–676, 2021
https://doi.org/10.1007/s11998-020-00431-3

A novel approach for the evaluation of ice release performance of coatings using static friction measurements

M. Martinsen, K. O. Hed, J. S. Diget, H. L. Lein

Received: 11 November 2019 / Revised: 25 September 2020 / Accepted: 30 September 2020

Abstract Atmospheric icing on structures and equipment represents a challenge for operation and safety. Passive ice removal by ice-phobic coatings has received much attention over the last decades. The current state-of-the-art methods for quantifying the ice-release properties of such coatings suffer from a range of drawbacks, including poor reproducibility and high complexity test setups. Here, a facile rotational tribometer approach for measuring the static friction between polymeric coatings and ice is presented. The torque necessary to initiate motion at the coating-ice interphase was used as a measure of ice release. For a polydimethylsiloxane-based coating (Sylgard 184), the effects of ice-temperature, normal force, coating thickness, and dwell time (contact time between coating and ice at rest with fully applied normal force prior to applying torque) were established along with the conditions resulting in least data variation. With these conditions, tribology-based friction measurements were carried out on two additional coatings; a two-component polyurethane, and a commercial foul release coating. The outcome of the method, i.e., grading of the coatings in terms of antiicing effect, matched those obtained with a widely used ice adhesion test method based on ice shear adhesion testing. The same trends are revealed by the two methods. However, the findings from the proposed tribology-based method result in consistently lower variation in outcomes and offer more detail on the ice adhesion and friction mechanisms.

Keywords Ice adhesion, Static friction, Ice shear strength, Friction on ice

Introduction

Ice accumulation on surfaces in cold climates represents a serious challenge from an operational, economical, and safety perspective. A prominent example of this is the ice accumulation on wind turbine blades, resulting in either impaired function, malfunction or shutdown of the turbines, along with the risk of ice fall and ice throw from the wind turbines.[1,2] Atmospheric and sea-spray icing on life rafts and walkways of ships and offshore installations are other examples where icing poses a serious safety risk.[3] Therefore, the development of antiicing and ice release coatings has been a subject of great interest over the last decades.[4–8] Due to the large scale of real-life applications, the development of such coatings commonly relies on a range of in-laboratory test methods performed under controlled conditions.

Jellinek et al.[4] describe a shear stress apparatus used to detach a block of ice from a flat horizontal surface, yielding a measure of the shear force for ice removal. In this experimental setup, a hollow aluminum mold is placed on a panel coated with a polymeric coating and the mold is filled with water and frozen onto the coating. A pressure gauge is used to measure the peak force obtained when removing the ice from the surface. This methodology, or adaptations thereof, has been frequently adopted in the evaluation of ice adhesion.[9–11] Advantages include ease of sample prepara-

Electronic supplementary material The online version of this article (https://doi.org/10.1007/s11998-020-00431-3) contains supplementary material, which is available to authorized users.

M. Martinsen (✉), H. L. Lein (✉)
Department of Materials Science and Engineering, Norwegian University of Science and Technology, Sem Sælands Vei 12, 7491 Trondheim, Norway
e-mail: morten.martinsen@jotun.no

H. L. Lein
e-mail: hilde.lea.lein@ntnu.no

M. Martinsen, K. O. Hed, J. S. Diget
Jotun A/S, Hystadveien 167, 3209 Sandefjord, Norway

tion, low complexity test setup, and high throughput. It has, however, been shown that factors such as the shape and material of the mold [12] and probe position [10] impact the results. Hence, the direct comparison between results obtained from different equipment is challenging. Another popular method generating comparable results is the centrifugal ice adhesion test (CAT) developed by the Anti-icing Material International Laboratory (AMIL).[13] As the name implies, ice is sheared from a test substrate by means of centrifugal forces. Rønneberg et al. [14] showed, using the CAT setup, that different types of ice produced significantly different ice shear results. Test setups with ice removal by pressurized air have also been described.[15–17] The latter two test methods permit simulation of different icing scenarios such as freezing drizzle or atmospheric icing, albeit with more complex and rigorous test setups, resulting in low accessibility for most developers.

Thus, there is a need for an easily accessible high throughput method offering both high levels of reproducibility and giving a better understanding of ice release mechanisms.

In the present study, a rotational tribology approach to ice adhesion was explored as a potential technique fulfilling these needs. A rotational tribometer offers high accuracy control of the normal and frictional forces at the coating-ice interphase and is widely available.[18,19] Tribometers have been used to measure frictional forces between ice and polymeric materials in the past for many materials.[20–24] However, the focus has been on the sliding friction for areas such as rubbers for the tire industry. The correlation between ice adhesion and the break-away torque has not previously been investigated, where the latter is defined as the minimum amount of torque necessary to initiate macroscopic motion between a coated surface and ice. In this work, the break-away torque between ice and coatings was investigated using a rotational tribometer. Via a design of experiments approach, the most significant parameters affecting the ice release properties of a commercial PDMS coating were found, along with test conditions resulting in the highest reproducibility. With these test conditions, results obtained for three representative coatings were compared with those obtained using a conventional shear stress approach by Jellinik et al. and revealed the same grading in terms of antiicing effect of the coatings. Detailed information about the frictional behavior of the three coatings was furthermore obtained by measuring the dynamic friction over a range of sliding velocities (Stribeck-curves).

Experimental

Materials

Butyl methacrylate (BMA), hydroxy ethyl methacrylate (HEMA, 97%), 2,2′-azodi(2-methylbutyronitrile) (AMBN, ≥ 98%) were purchased from Sigma-Aldrich. Xylene (≤ 25% ethyl benzene) was purchased from Brenntag Nordic AS. Tetrahydrofurane (THF, ≥ 99.8%) was purchased from VWR. Isophorone diisocyanate trimer (IPDI trimer in 30 wt% butyl acetate, Desmodur Z 4470 BA) and hexamethylene diisocyanate biuret (HDI biuret in 25 wt% 1-methoxypropylacetate/xylene, 1:1, Desmodur N75 MPA/X) were purchased from Covestro AG. Dioctyltin dilaurate (DOTDL, 95%) was purchased from TIB Chemical AG. All reagents were used as received. Penguard Universal (epoxy primer), Sea Lion tie-coat (silicone tie-coat), and Sea Lion Repulse (condensation cured silicone foul release coating) were supplied by Jotun A/S with technical datasheets and application guides available through www.jotun.com. Wacker primer G 790 was purchased from Wacker Chemie AG and Sylgard 184 (Dow Corning) from Sigma-Aldrich, with technical datasheets and application guides available through www.wacker.com and www.sigmaaldrich.com, respectively.

Chrome steel beads (100Cr6, Ø 6 mm) were purchased from Rotek AS. Aluminum panels (1050A, 1.5 mm thickness) were purchased from Erling Freitag AS. Mylar® polyester film (19 μm thickness) was purchased from Arcon AS.

Analytical methods

Gel permeation chromatography (GPC) was carried out at 30°C on a Malvern Omnisec GPC system with a PL-gel 5 μm Mixed – D column (Polymer Labs), THF as mobile phase and with a flow of 1 mL/min. Absolute molar masses were detected using a low- and right-angle light scattering detector (LALS/RALS) with a 640 nm laser source. Values for dn/dc_w were determined using a differential refractive index detector, which was also used for concentration monitoring. Linear polystyrene standards were used for calibration of the light scattering detectors. Water contact angle (WCA) measurements were carried out on a Krüss DSA100 drop shape analyzer with 2 μL drop size of distilled water at 23°C and 50% relative humidity (RH). Stress–strain curves were obtained using a universal testing machine (UTM) from Testometrics Co. Ltd. at a pull rate of 5 mm/min at 23°C according to ASTM D638-14.[25] Static and dynamic friction measurements were carried out on an Anton Paar MCR-302 rheometer fitted with a pin-on-disk T-PID/44 tribology system, H-PTD 200 Peltier Hood and P-PTD200/80/I Peltier cooling plate.

Synthesis of polyacrylic polyol

For the 2-component polyurethane (2K PU), a polyacrylic polyol was synthesized. Synthesis was carried out in a 250 mL four-necked round-bottomed flask, equipped with a mechanical stirrer, a condenser and

thermocouple, with nitrogen flow throughout the reaction.

Xylene (40.0 g) was added, and the temperature was increased to 90°C. A mixture of BMA (80.0 g, 563.0 mmol), HEMA (20.0 g, 154.0 mmol), AMBN (4.7 g, 24.5 mmol), and xylene (60.0 g) was added dropwise over 2 h. Following addition, the reaction mixture was stirred for a consecutive 30 min, after which AMBN (0.3 g, 1.6 mmol) in xylene (3.0 g) was added as chaser. After 90 min, the reaction was cooled to ambient temperature. The resulting 50 wt% polymer solution was used without further purification. GPC data: weight average molar mass (M_w) = 21,440 g/mol, dispersity (Đ) = 2.24.

Coating preparations

For all commercial coatings, application was carried out following the technical datasheets and application guides referred to in the "Materials" section. Examples, including application of the 2K PU coating, are given below, and further details about the materials, coating application, and curing conditions can be found in the supplementary information (Table S1). All coatings were mixed and applied at room temperature and 30–50% RH.

Chrome steel beads were used as substrate for the break-away torque experiments. The beads were cleaned by immersion in xylene, dried, and held into position on a flat surface by using a magnet. Finally, the beads were coated with a primer coat (Wacker primer G 790) using a conventional spray gun (1.6 mm nozzle, no. 510 + aircap, approx. 2 bar inlet pressure, Devilbiss Advance HD). The primer coat was cured for 2 h at ambient temperature. Sylgard 184 base resin and Sylgard 184 hardener were mixed (10:1 parts by weight) using a speedmixer (Speedmixer™ DAC 600.1 FVZ) at 2300 rpm for 1 min. Immediately following mixing, the paint was applied onto the primed steel beads using conventional spray (the same apparatus and settings as used for the primer coat). As reference, a flat aluminum panel was coated alongside the beads with the same distance to the paint nozzle. The beads and the aluminum reference panels were cured at ambient temperature for 24 h followed by 80°C for 2 h. After curing, the beads were held in position by the coating itself. The dry film thicknesses (DFTs) were measured with a coating thickness gauge (Positector 6000) according to standard ISO 2360:2017 on the aluminum reference panels, and the DFT was assumed to be the same for the steel beads and the aluminum reference. By assuming that the paint settles equally on the flat panel and the small part of the bead in contact with the ice, measurement of the DFT of the flat metal panel should equal that of the beads.

The foul release coating, Sea Lion Repulse, was prepared by mixing the base formulation (component A) with crosslinker (component B) and catalyst (component C) (A: B: C = 17: 0.7: 0.75 parts by volume) and applied onto chrome steel beads previously coated with a primer- and tie-coat (Penguard Universal primer and Sea Lion tie-coat, respectively) in a similar manner as above.

The 2-component polyurethane (2K PU) coating was prepared by mixing the polyacrylic polyol synthesized as explained in the "Synthesis of polyacrylic polyol" section (200 g of the crude polymer solution composed of 50 wt% polymer in xylene) with DOTDL (0.02 g, 0.027 mol), followed by mixing with an isocyanate curing agent mixture (18.3 g HDI biuret + 27.3 g IPDI trimer) with an overall isocyanate to hydroxyl molar ratio of 1.1: 1. Immediately after mixing, the coating was applied in a similar manner as described for Sylgard 184.

For the ice shear stress test, aluminum panels (75 × 100 × 1.5 mm) were used as substrate. The panels were lightly abraded with P150 sandpaper and washed with xylene. Coating was applied using a bar-applicator, and the DFT was measured for the individual panels using a coating thickness gauge (Table S2). The panels coated with 2K PU and Sea Lion Repulse were cured at 23°C/50% RH for 1 week prior to ice adhesion testing. The panels coated with Sylgard 184 were cured as described above. The mechanical and surface-properties of the coatings are summarized in Table 1. The relationship between the properties reported in Table 1 is not expected to change significantly within the testing temperature range (− 20°C to 23°C) as no phase transitions occur for the polymeric binders of the coatings.

Break-away torque and sliding friction measurements

A rotational rheometer (Anton Paar MCR-302) with a pin-on-disk tribology-fixture with three points of contact to the substrate was employed (depicted in Fig. 1). The rheometer was fitted with a Peltier cooling plate to control the temperature of the ice and a cooling hood to control the temperature of the surroundings. The temperature of the ice and air was kept equal during the test. Three equally coated beads were inserted into the tribology fixture sample holder for each measurement. This was done to avoid variation between measurements due to wear of the coating.

Ice surfaces were premade by pouring 6.5 mL distilled water into silicone molds (d = 60 mm, thickness = 2 mm) and covered with a Mylar® polyester film to obtain planar surface topography and kept at − 18°C for at least 3 h. A premade ice disk (as shown in Fig. 1) was then transferred to the rheometer, kept at the desired analysis temperature, and allowed to equilibrate for 15 min.

A typical break-away torque experiment, exemplified by run 1 in Table 3, was carried out by first lowering the sample beads onto the ice (− 20°C) and stabilizing the normal force. To ensure the same running conditions for all samples, the sample fixture

Table 1: Mechanical properties and static WCA of the test coatings at 23°C

Coating	Young's modulus (MPa)[a]	Ultimate tensile strength (MPa)[a]	Static WCA (°)
2K PU	724	22	84
Sea Lion Repulse	0.5	0.7	105
Sylgard 184	3.09	4.92	110

[a] Extracted from stress–strain curves obtained using a UTM. The Young's modulus for Sylgard 184 is slightly higher than expected from literature [26] which is due to different curing conditions and testing methods

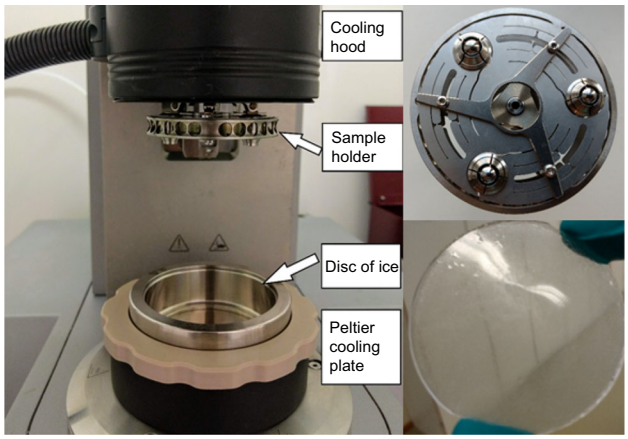

Fig. 1: Pin-on-disk experimental setup. The instrument (left) fitted with cooling hood and Peltier cooling plate where a disk of ice is mounted, the pin-on-disk sample holder (upper right) with three beads coated with Sylgard 184 (transparent) which is lowered onto the disk of ice and an example of a premade disk of ice (bottom right)

was rotated at a constant speed and normal force (20 rpm, 1 N) for 15 s (running in step) prior to a dwell time (5 min) at rest with constant normal force (0.3 N). During this step, a liquid boundary layer of water is formed which refreezes upon motion stop during the dwell time. The sliding distance was then recorded by logarithmically increasing the torque from 0.1 mN·m to 100 mN·m with 123 points per decimal while maintaining a constant temperature and normal force.

The Stribeck curves were obtained in a similar manner as the break-away torque without a running in- and dwell time-step. The rotational speed was increased logarithmically from 10^{-6} rpm to 10^{3} rpm with constant normal force and temperature. More details of the test protocol can be found in the supporting information.

Ice shear test

Ice shear stress was measured using a UTM fitted with a 50 kg load cell and a climate chamber (temperature range − 40 to 200°C) both from Testometrics Co. Ltd. A custom-made fixture was employed, containing a locking position for the coated aluminum test panels with an off-set in a horizontal direction, deflecting the normal force into a shear force pulling a mold wherein ice had been formed on the coated aluminum panel. The molds were 3D printed with polylactic acid (PLA Extrafill, Fillamentum) with an inner diameter of 20 mm, wall thickness 3 mm, and tracks for mounting the wire 3.5 mm from the substrate.

The mold, placed on the coated aluminum panel, was filled with distilled water and frozen at – 18°C for 24 h. Prior to starting the test, the test setup was equilibrated at – 10°C in the climate chamber for 1 h. Each sample (mold with ice on coated aluminum panel) was moved quickly from freezer to the instrument and allowed to equilibrate for 5 min before starting the test.

The mold (and thus water frozen onto the coating) was pulled by a fixed pulley via a wire (Dubro 4-40 pull–pull) attached to the load cell at a constant speed of 10 mm/min until an adhesive break between the ice and the coating occurred, and the peak force was recorded. See Fig. 2 for a depiction of the setup, example of a shear curve obtained using the method, and the PLA mold.

Experimental design

JMP® statistical software (SAS Institute) was used for the design setup and analysis of results. Normal force, temperature, coating thickness, and dwell time were defined as the factors and break-away torque as the single response. Response surface methodology (RSM) was used to find interactions between the factors. The ranges in which the parameters were varied are based on previous reported values.[20,27,28]

The custom design function in JMP® was used for the design setup with the design space given in Table 2. The coating thickness was handled as a discrete numeric value for practical reasons.

A total of 21 experiments were carried out according to the testing variables given in Table 2. Each experiment was performed twice in a random order to avoid systematic errors. The ambient temperature outside the test chamber was constant at 23°C, and the RH in the test chamber was approximately 100% at all test temperatures given in Table 2.

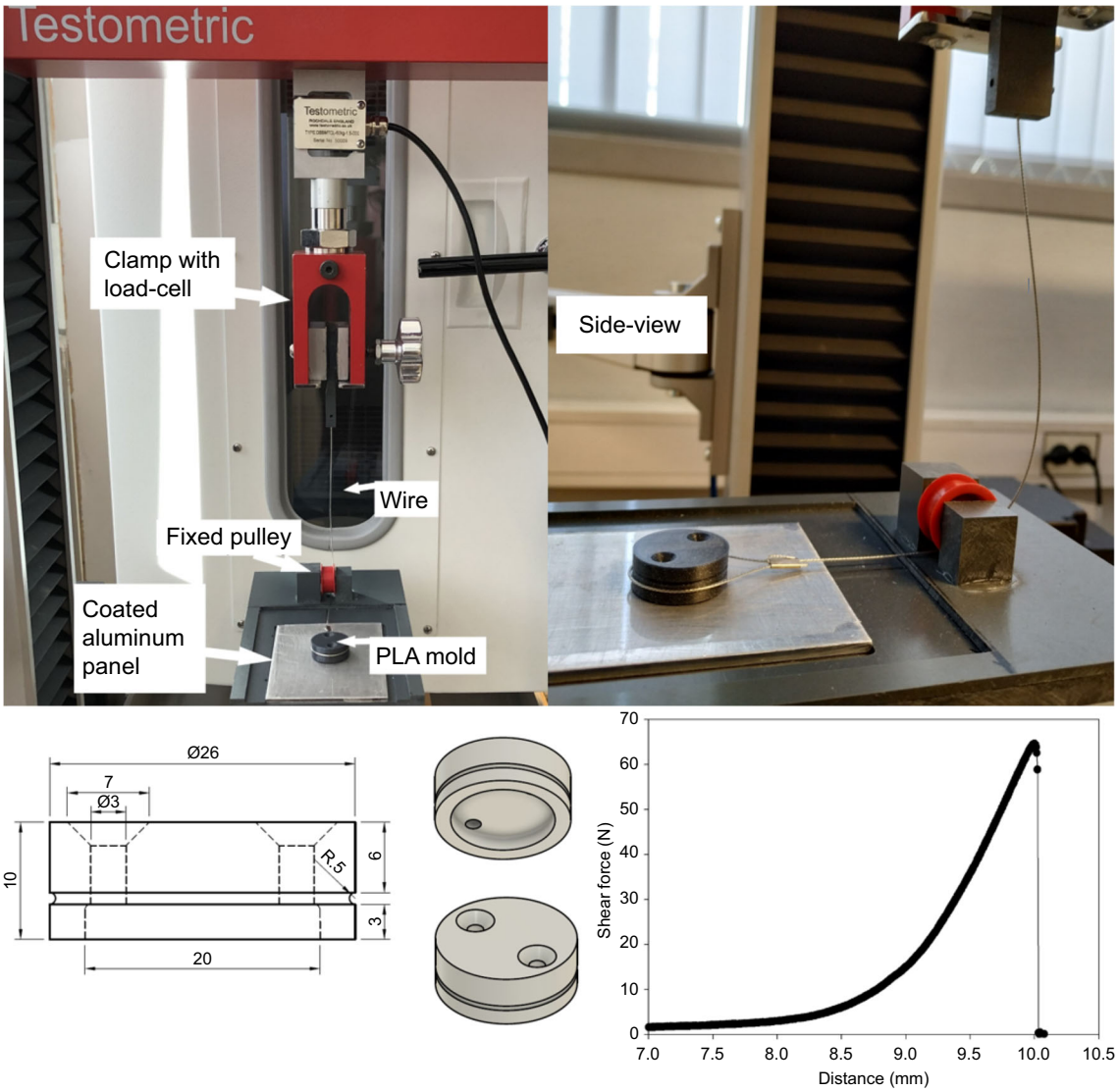

Fig. 2: Ice shear strength experimental setup. To the upper left: A PLA mold is filled with water and frozen onto an aluminum panel coated with Sylgard 184. A wire with a loop is attached to the PLA mold, and the other end of the wire is attached to a clamp. Upper right: Side view of instrumental setup. The experimental setup is photographed outside of the climate chamber for clarity. Lower left: Model of 3D-printed PLA mold (top- and bottom-view including dimensions) with tracks to attach the wire and holes at the top to fill water and for the ice/water to expand upon freezing. The inside of the mold is hollow and open in the bottom for the water/ice to touch the coating surface. Lower right: Example of peak force when removing the mold from the substrate

Table 2: Defined factors and design space

Factor	Role	Measured levels
Temperature (°C)	Continuous	− 20, − 12.5, − 5
Normal force (N)	Continuous	0.3, 1.15, 2
Dwell time (min)	Continuous	5, 32.5, 60
Coating thickness (μm)	Discrete numeric	66, 122

Results and discussion

Determining the break-away torque

The measurements of break-away torque between ice and three chemically different commercial coatings are presented in Fig. 3 (conditions given in figure text). The figure illustrates how such measurements can be used to compare ice release properties of coatings. The sliding distance between the fixed ice disk and the rotating specimen holder shows initial small movement in the low torque region, followed by a sudden leap in sliding distance once the torque reaches a critical level. The onset of the rapid movement indicates initiation of motion and is defined as the break-away torque. A different degree of sliding distance prior to the break-away point is observed for the three coatings as an effect of the differences in elastic modulus and thickness of the coatings. The onset point is used as a measure of ice release property of the coatings throughout the work and was found as the intersection of the tangent lines before and after motion was initiated (as shown in Fig. 3). Sea Lion Repulse has a break-away torque around 0.43 ± 0.06 mN·m, indicating superior ice release as compared to Sylgard 184 and 2K PU reaching this point at 5.7 ± 0.4 mN·m and 15.34 ± 1.7 mN·m, respectively (from three measurements). Testing of all three coating systems was carried out with a start torque of 0.1 mN·m. For Sea Lion Repulse, testing was also carried out with a start torque of 0.05 mN·m (used for depiction in Fig. 3) as it turned out that the onset point was close to 0.1 mN·m. Thus, 0.05 mN·m resulted in more precise break-away torque values. Sea Lion Repulse has a different curve development than the two other coatings, with a less sharp transition from stationary to motion because of the low break-away torque and modulus of the coating. Sylgard 184 and the 2K PU are both less elastic and have a significantly higher break-away torque than Sea Lion Repulse, which results in a sharper transition between stationary and motion.

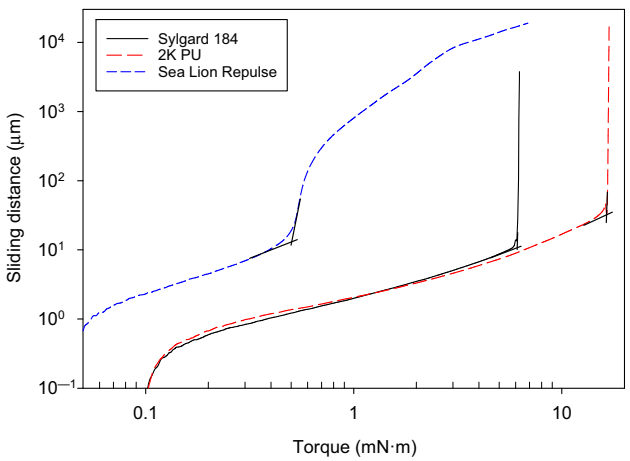

Fig. 3: Sliding distance between a fixed disk of ice and rotating specimen holder for Sylgard 184, 2K PU, and Sea Lion Repulse coating samples. Conditions: T = − 10°C, F (normal) = 1 N, dwell time = 5 min. Start torque of Sea Lion Repulse of 0.05 mN·m and 0.1 mN·m for Sylgard 184 and 2K PU

Influence of temperature, normal force, dwell time, and coating thickness on break-away torque

The motivation for using a design of experiments approach was to determine the impact of the measurement parameters on the break-away torque, and to indicate which parameter settings resulting in least variation of repeated measurements. Only the coating system with Sylgard 184 was used in these experiments for which parameter settings, as proposed by the JMP software and explained in the ''Experimental design'' section, are given in Table 3.

In the same table, break-away torques are given as the average of the two measurements carried out per experimental parameter, and standard deviation (SD) of those measurements. Prior to preparing a predictive model from the results, a jackknife analysis was carried out to determine potential outliers.[29] Three measurements were identified as potential outliers and thus excluded from the model, resulting in 39 datapoints.

The standard least squares linear regression in JMP resulted in the following linear regression model:

$$y = 8.26 - 0.46T + 4.40F + 0.55t + 0.54CT - 0.7T^2 - 0.51(T * F) - 1.38F^2 + 0.61(T * t) + 0.48(t * CT) \quad (1)$$

where y is the break-away torque, T the temperature, F the normal force, t the dwell time and CT the coating thickness. The parameter terms (T, F, t and CT) are scaled as shown in equation 2 where the levels H (high level) and L (low level) correspond to the low and the high values of the parameter, e.g., −5°C and − 20°C, respectively, for the temperature-parameter and ''parameter'' is the actual value.

$$Parameter\ term = \frac{Parameter - \frac{H+L}{2}}{\frac{H-L}{2}} \quad (2)$$

The summary of fit produces a high coefficient of determination (R^2) and low root mean square error (RMSE), indicating that the model is suitable for predicting break-away torque in the design space (Table 4), i.e., within values given in Table 3 for the Sylgard 184 coating system.

Temperature, normal force, freezing time, and coating thickness were all found to be significant factors with a P value < 0.05 (Student's t-test, null hypothesis is that the true value for each parameter is zero). In Fig. 4, the effect of each significant parameter

Table 3: Results from the design of experiments with experimental parameters where break-away torque is given as an average of two measurements carried out on the Sylgard 184 coating system

Run#	Temperature (°C)	Normal force (N)	Dwell time (min)	Coating thickness (μm)	Break-away torque (mN·m)	SD (mN·m)
1	− 20	0.3	5	122 ± 6	1.735	0.265
2	− 20	0.3	32.5	66 ± 5	1.685	0.205
3	− 20	1.15	60	66 ± 5	7.16	0.5
4	− 20	1.15	60	122 ± 6	8.2	0.52
5	− 20	2	5	66 ± 5	11.58	1.32
6	− 20	2	32.5	122 ± 6	12.26	0.21
7	− 12.5	0.3	32.5	66 ± 5	1.615	0.115
8	− 12.5	0.3	60	122 ± 6	3.845	0.085
9	− 12.5	1.15	5	66 ± 5	6.935	0.905
10	− 12.5	1.15	5	122 ± 6	7.225	0.285
11	− 12.5	1.15	32.5	66 ± 5	8.11	0.76
12	− 12.5	1.15	32.5	122 ± 6	10.295	1.375
13	− 12.5	1.15	32.5	122 ± 6	8.855	0.085
14	− 12.5	2	60	66 ± 5	14.74	4.21
15	− 5	0.3	5	66 ± 5	1.075	0.015
16	− 5	0.3	32.5	122 ± 6	2.36	0.28
17	− 5	0.3	60	66 ± 5	1.665	0.155
18	− 5	1.15	32.5	66 ± 5	6.435	0.305
19	− 5	2	5	122 ± 6	8.305	0.195
20	− 5	2	32.5	66 ± 5	15.5	6.3
21	− 5	2	60	122 ± 6	16.58	4.58

Table 4: Summary of fit

R^2	0.96
R^2 adjusted	0.95
RMSE	0.86
Mean of response	6.42
Observations[a]	39

[a]A total of 42 experiments, 21 experiments with double determination, were carried out where three experiments were identified as outliers from a jackknife analysis and thus excluded from the regression model

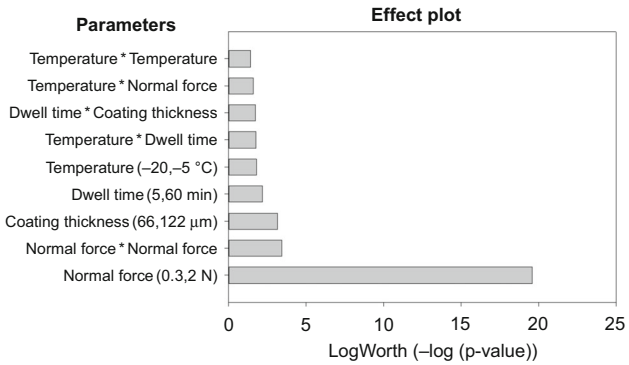

Fig. 4: Effect plot of main parameters and significant interactions

is plotted as the -log (p-value) visualizing the relative parameter impact on break-away torque.

As directly seen from the effect plot, the applied normal force has the highest contribution on the break-away torque. This can be explained by the increased contact area between the coating and ice when increasing the normal force. The contact area between a sphere and a planar surface can be expressed as follows[30]

$$a = \left(\frac{3WR'}{E'}\right)^{\frac{1}{3}} \tag{3}$$

where α is the radius of the circular contact area, W the applied normal force, R' the radii of curvature, and E' the reduced Young's modulus, which is a function of the Poisson's ratio and Young's moduli of the contacting bodies. From equation (3), it follows that both increased normal force and reduced Young's modulus will increase the area of contact and the effect plot in Fig. 4 indicates that normal force is the most important parameter to control when measuring break-away torque.

Figure 5 gives a visualization of parameter interactions from the linear regression model (equation 1) as predicted by the JMP software. The y-axis of each square shows how the break-away torque is dependent on the main parameters: temperature, normal force, dwell time, and coating thickness.

The break-away torque is significantly lower at temperatures closer to – 5°C and high normal force than at lower temperatures and high normal force (Figs. 5a and 5d). This indicates more water in the boundary for the temperatures closer to – 5°C than for the experiments carried out at temperatures closer to – 20°C. There is also a significant increase in break-away torque for long dwell times and low temperatures which again indicates more water at the boundary with increasing temperature of the ice (Figs. 5b and 5g). Longer dwell times will allow more of the boundary water to freeze and thus increase the break-away torque.

The break-away torque increases with increasing coating thickness and dwell times (Figs. 5i and 5l). Sylgard 184 has a Young's modulus between 1.32 and 2.97 MPa depending on curing conditions[26] and is a soft material with glass transition temperature well below the temperatures used in this test. The increased coating thickness of the relatively soft Sylgard 184 will increase the real contact area to the ice and thus give increased break-away torque. This is in alignment with the findings of Blackford et al.[20] that rigid materials (steel) have lower static friction than the lower elastic modulus materials (polymethylmethacrylate) on ice. The bulk modulus of Sylgard 184 on steel substrate (beads) will be affected by the coating thickness. However, it is interesting to note that when measuring ice shear strength on a planar surface of an elastic coating, the ice adhesion is reduced with increased coating thickness because of the deformation of the coating when stress is applied, and ice more easily shed off the surface.[28]

Reproducibility of break-away torque measurements for Sylgard 184

The reproducibility of the model obtained from the statistical software was evaluated by using replicated points as part of residual error (lack of fit test). Good reproducibility is indicated by p-value = 0.4845 (> 0.05, i.e., there is no significant lack of fit).

The lowest SD is found for measurements with normal force ≤ 1.15 N (Fig. 6). Measurements at normal force > 1.5 N have less reproducibility. The

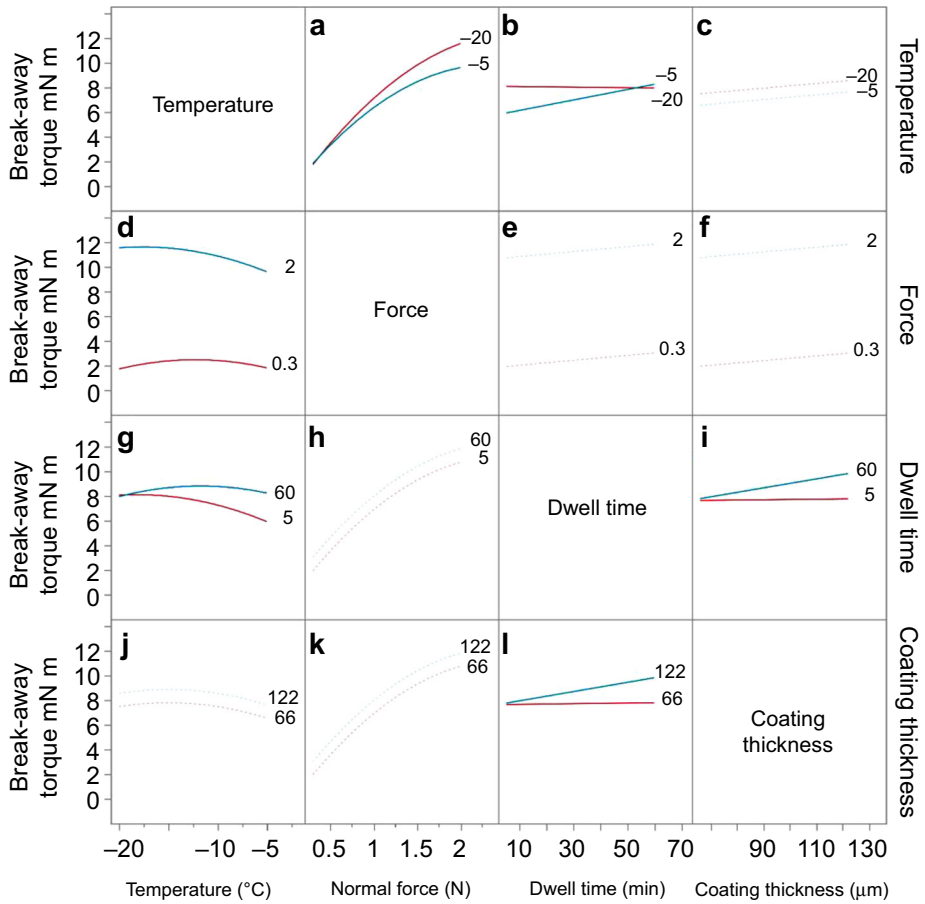

Fig. 5: Visualization of parameter interactions where dotted lines indicate no significant interactions and solid lines indicate significant interactions. The torque is given on the left y-axis for each subplot. The interaction parameters are given on the x-axis and right y-axis, with values of the former given on the axis and values of the latter given in each subplot as the two numbers

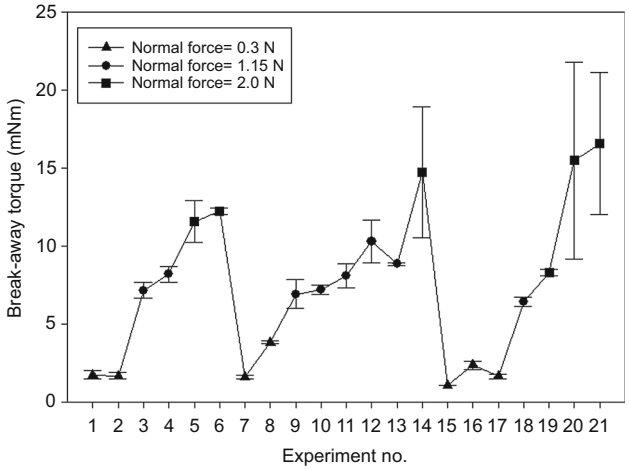

Fig. 6: Break-away torque (y-axis) for the various experiments on Sylgard 184 (indexed on the x-axis) with normal forces indicated by symbols. Each datapoint represents the average with SD of the two measurements carried out per experimental condition

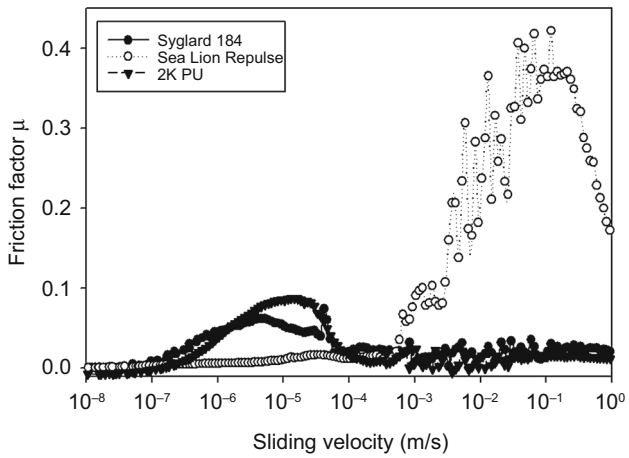

Fig. 7: Stribeck curves with sliding velocities from 10^{-8} m/s to 1 m/s as a comparison between Sylgard 184 (DFT = 122 μm), Sea Lion Repulse (DFT = 81 μm) and 2K PU (DFT = 50 μm). T = − 10°C, F (normal) = 1 N

data from which the model is constructed only have few datapoints in this region as some datapoints were identified as outliers, using the jackknife analysis as described above, and thus removed thereby also resulting in lower reproducibility > 1.5 N. The large variation in the experiments carried out at high normal force might be explained by inconsistent amounts of water in the ice-coating boundary. The Hertzian contact pressure cannot be directly applied for the sample specimen as the elastic modulus of the thin coating films will be affected by the steel substrate, though it is evident that increased normal force affects the reproducibility of the measurements.

The linear regression model (equation 1) obtained from the data in Table 3 was validated by a set of separate experiments where the parameters were chosen randomly within the design space. Ninety-two percent of the experiments fit with the predicted values (95% confidence interval encompassing variation from predicted value and individual measurements). As expected, the experiments that did not match the predicted values were those carried out at high normal force. Further details about experimental parameters and break-away torques can be found in Table S3 in the supporting information.

Sliding friction

Stribeck curves offer insight into the frictional forces between two surfaces from the boundary lubrication through the hydrodynamic lubrication regime. The frictional forces are usually high because of direct contact between the asperities of two solids at low sliding speeds. Frictional heat and pressure melting at higher speeds form a lubricating layer of liquid water resulting in reduced friction between the surfaces.[31]

Foul release coatings typically contain some extent of free silicone oils that lubricate the surface. The presence of a lubricant oil in the ice-coating interphase might also result in reduced friction and adhesion, as previously shown for slippery liquid infused porous surfaces.[6] The dynamic friction was therefore measured to investigate potential lubrication from liquid water and/or silicone oils.

In Fig. 7, the friction factor μ is plotted as a function of sliding speed under the same conditions for the three coatings. As seen from Fig. 7, the data do indeed confirm that the Sea Lion Repulse coating (the foul release coating) has much lower friction up to 10^{-3} m/s compared to the two other coatings. This corresponds well with the extra lubrication from free silicone. In the high-speed domain (> 10^{-3} m/s), however, a significant increase in friction is observed for the Sea Lion Repulse only.

Mielonen et al.[24] observed higher sliding friction for soft materials than for harder materials (3.2 x 10^{-2} m/s sliding speed). As Sea Lion Repulse is a much softer material than the two other coatings, this explains the large increase in friction above 10^{-3} m/s sliding speeds. Sylgard 184 demonstrates a change from boundary lubrication to mixed lubrication/hydrodynamic lubrication for sliding speeds above 10^{-3} m/s.

It was only one run per dynamic friction measurement per sample due to wear of the samples. Replicate runs for samples coated via exactly the same approach and DFT showed the same trend. A few trials were conducted prior to the measurements where the test was stopped prior to rapid increase in friction (at approximately 10^{-3} m/s sliding velocity), and samples were evaluated under optical microscope. Up to this point, no macroscopic wear was observed. This also confirmed that no cohesive fracture or adhesive fracture between coating and steel-bead took place at these sliding velocities.

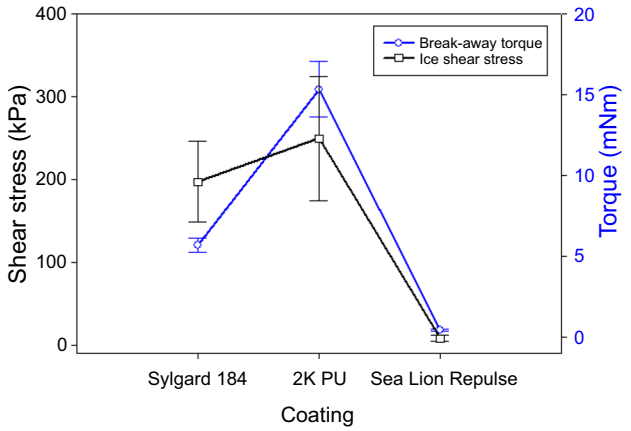

Fig. 8: Comparison between break-away torque and shear strength of ice where the shear stress in kPa is indicated on the left axis (black squares) and the break-away torque in mN·m is indicated on the right axis (blue circles). Break-away torque was measured at − 10°C, F (normal) = 1 N and dwell time = 5 min (average of three measurements). Shear stress was measured at − 10°C (average of five measurements)

Correlation between break-away torque and shear stress

Test conditions in the range that resulted in least variation in the break-away torque for Sylgard 184 (experiments with normal force < 1.15 N in Table 3) were used to compare break-away torque between Sylgard 184, a 2K PU coating and Sea Lion Repulse. The ice adhesion strength was also measured for these coatings by a conventional shear stress method, and Fig. 8 compares the break-away torque (mN·m) and shear strength adhesion (kPa).

As can be seen from the comparison of break-away torque and shear stress curves, the scaled SD of the shear strength measurements are three-fold greater than the scaled SD of the break-away torque measurements (for details, see Table S4 in the supporting information). Importantly, however, the trends of both test methods are similar with Sea Lion Repulse revealing the best ice release properties, followed by Sylgard 184 and the 2K PU coating with highest ice adhesion value. The coatings with low elastic modulus (Sea Lion Repulse and Sylgard 184) show lower ice adhesion in both tests compared to the 2K PU coating. As seen from the WCA results given in Table 1, it is moreover indicated that the former two coatings are more hydrophobic than the latter, which should also result in lower ice adhesion. However, the elasticity modulus and surface roughness must also be considered for a direct comparison.[31] The previous literature demonstrates that a large difference in elastic modulus between the ice and the coating, e.g., silicone rubbers, gives a reduction in ice adhesion strength.[32,33] This is also the case for the observed static friction measurements in Fig. 8.

The comparison of the developed break-away torque method and a conventional ice shear test for the three commercial coatings showed the same trend for break-away torque and shear strength. However, the uncertainty between Sylgard and the 2K PU coating in the ice shear test is so large that they can appear constant for this test method. For the break-away torque method, the uncertainties are much lower and indicate large difference between those two coatings. Both tests are laboratory screening tests as they measure ice adhesion on bulk-water ice. The static friction method measures the friction force (acting opposing to the shear force applied) necessary to initiate macroscopic motion between the contact-points. In the ice shear stress method, a shear force is applied on the mold of ice, where the obtained value might be affected by the force distribution on the mold itself or throughout the ice. Another obvious difference is the contact area where break-away torque is measured on a relatively small area, whereas the shear strength method measures ice adhesion on relatively large surface areas. The contact between the ice and coating in the developed method is different from ice prepared directly on the substrate, such as bulk-water ice, precipitation ice or in-cloud ice.[14]

Conclusion

The static and dynamic friction between Sylgard 184 and ice were explored under different conditions using a rotational rheometer-tribology approach. Applied normal force had the most significant effect on the break-away torque due to the increased contact area. However, the effects of temperature, dwell time, coating thickness and interactions were also found to be statistically significant. Long dwell time was important for experiments at temperatures closer to – 5°C and is most likely a result of a lubricating layer of water forming during the short dwell time experiments.

The in situ produced ice-coating interphase will depend on the surface roughness of both the ice and the coating and on the ‘‘running in’’ step (constant speed and normal force are applied for some seconds). The running in step, carried out prior to actual measurements, worked to give a normalized starting point for measurements. The liquid boundary layer of water formed during this step refreezes upon motion stop during the dwell time. Sufficient dwell time and dwell temperature were found to be important to reduce measurement variation and allow complete refreezing of this boundary layer. The real contact area between the ice/coating and the presence and importance of liquid water in the interphase are topics for further investigation.

The commercial foul release coating, Sea Lion Repulse, revealed a magnitude lower ice adhesion compared to Sylgard 184 and the 2K PU coating in both break-away torque and shear stress. Furthermore,

the foul release coating showed low sliding friction in the dynamic friction experiments. The findings confirm that hydrodynamic lubrication at low sliding velocities is important to achieve low ice adhesion materials. Importantly, measurement of ice adhesion in terms of static friction correlates well with the previously described ice shear strength method, gives improved reproducibility of each measurement and Stribeck curves offer insight in the frictional forces between ice-coating interphase under static and dynamic conditions.

The methodology presented is highly attractive as it offers a standardization of ice adhesion measurements making comparison across laboratories much more reliable. This was achieved by employing a widely available rotational tribometer without the need for custom modifications.

Acknowledgments Financial support from Jotun A/S and the Research Council of Norway (Grant No. 291637) is gratefully acknowledged. The authors would also thank Bjørn Haavaldsen and Thor Haakon Krane Tvedt for designing a test rig for the shear strength apparatus and 3D-printing of molds.

Funding Open Access funding provided by NTNU Norwegian University of Science and Technology (incl St. Olavs Hospital - Trondheim University Hospital).

References

1. Karthikeyan, N, Anand, RB, Suthakar, T, Barhate, S, ''Materials, Innovations and Future Research Opportunities on Wind Turbine Blades—Insight Review.'' *Environmental Progress & Sustainable Energy*, **38** (3) e13046 (2019). https://doi.org/10.1002/ep.13046
2. Krenn, A, Stökl, A, Weber, N, Barup, S, Weidl, T, Hoffmann, A, Bredesen, RE, Lannic, M, Müller, S, Stoffels, N, Hahm, T, Storck, F, Lautenschlager, F, ''International Recommendations for Ice-Fall and Ice-Throw Risk Assessments.'' Wind Energy in Cold Climates (2018).
3. Ryerson, CC, ''Ice Protection of Offshore Platforms.'' *Cold Regions Sci. Technol.*, **65** (1) 97–110 (2011). https://doi.org/10.1016/j.coldregions.2010.02.006
4. Jellinek, HHG, Kachi, H, Kittaka, S, Lee, M, Yokota, R, ''Ice Releasing Block-Copolymer Coatings.'' *Colloid and Polym. Sci.*, **256** (6) 544–551 (1978). https://doi.org/10.1007/BF01639199
5. Andersson, LO, Persson, S, Golander, CG, Ice Accretion and Ice Adhesion to Polymer Materials. Luleå University of Technology (1993)
6. Kim, P, Wong, T-S, Alvarenga, J, Kreder, MJ, Adorno-Martinez, WE, Aizenberg, J, ''Liquid-Infused Nanostructured Surfaces with Extreme Anti-Ice and Anti-Frost Performance.'' *ACS Nano*, **6** (8) 6569–6577 (2012). https://doi.org/10.1021/nn302310q
7. Upadhyay, V, Galhenage, T, Battocchi, D, Webster, D, ''Amphiphilic Icephobic Coatings.'' *Prog. Org. Coat.*, **112** 191–199 (2017). https://doi.org/10.1016/j.porgcoat.2017.07.019
8. Golovin, K, Dhyani, A, Thouless, MD, Tuteja, A, ''Low–Interfacial Toughness Materials for Effective Large-Scale Deicing.'' *Science*, **364** (6438) 371–375 (2019). https://doi.org/10.1126/science.aav1266
9. Dong, W, Ding, J, Zhou, ZX, ''Experimental Study on the Ice Freezing Adhesive Characteristics of Metal Surfaces.'' *J. Aircraft*, **51** (3) 719–726 (2014). https://doi.org/10.2514/1.C032393
10. Wang, C, Zhang, W, Siva, A, Tiea, D, Wynne, KJ, ''Laboratory Test for Ice Adhesion Strength Using Commercial Instrumentation.'' *Langmuir*, **30** (2) 540–547 (2014). https://doi.org/10.1021/la4044254
11. He, Z, Vagenes, ET, Delabahan, C, He, J, Zhang, Z, ''Room Temperature Characteristics of Polymer-Based Low Ice Adhesion Surfaces.'' *Sci Rep*, **7** 42181 (2017). https://doi.org/10.1038/srep42181
12. Beeram, PSR, Waldman, RM, Hu, H, ''Measurements of Ice Adhesion over Ice Mitigation Coatings Pertinent to Aircraft Icing and Anti-/De-Icing.'' 9th AIAA Atmospheric and Space Environments Conference (2017). https://doi.org/10.2514/6.2017-3928
13. Laforte, C, Blackburn, C, Perron, J, ''A Review of Icephobic Coating Performances over the Last Decade.'' *SAE International*, (2015). https://doi.org/10.4271/2015-01-2149
14. Rønneberg, S, Laforte, C, Volat, C, He, J, Zhang, Z, ''The Effect of Ice Type on Ice Adhesion.'' *AIP Advances*, **9** (5) 055304 (2019). https://doi.org/10.1063/1.5086242
15. Andrews, EH, Majid, HA, Lockington, NA, ''Adhesion of Ice to a Flexible Substrate.'' *J. Mater. Sci.*, **19** (1) 73–81 (1984). https://doi.org/10.1007/BF02403112
16. Yeong, YH, Milionis, A, Loth, E, Sokhey, J, Lambourne, A, ''Atmospheric Ice Adhesion on Water-Repellent Coatings: Wetting and Surface Topology Effects.'' *Langmuir*, **31** (48) 13107–13116 (2015). https://doi.org/10.1021/acs.langmuir.5b02725
17. Janjua, ZA, Turnbull, B, Choy, K-L, Pandis, C, Liu, J, Hou, X, Choi, K-S, ''Performance and Durability Tests of Smart Icephobic Coatings to Reduce Ice Adhesion.'' *Appl. Surf. Sci.*, **407** 555–564 (2017). https://doi.org/10.1016/j.apsusc.2017.02.206
18. De Moerlooze, K, Al-Bender, F, Van Brussel, H, ''An Experimental Study of Ball-on-Flat Wear on a Newly Developed Rotational Tribometer.'' *Wear*, **271** (7–8) 1005–1016 (2011). https://doi.org/10.1016/j.wear.2011.01.027

19. Lauger, JPKS, New Insights into the Use of a Rotational Rheometer as Tribometer. *Annual Trans. Nordic Rheol. Soc.*, **25** (2017).
20. Blackford, JR, Skouvaklis, G, Purser, M, Koutsos, V, ''Friction on Ice: Stick and Slip.'' *Faraday Discussions*, **156** 243–254 (2012). https://doi.org/10.1039/C2FD00128D
21. Makkonen, L, ''Application of a New Friction Theory to Ice and Snow.'' *Annals of Glaciology*, **19** 155–157 (1994). https://doi.org/10.3189/1994AoG19-1-155-157
22. Bowden, FP, Hughes, TP, ''The Mechanism of Sliding on Ice and Snow.'' *Proceedings of the Royal Society of London. Series A, Mathematical and Physical Sciences*, **172**(949), 280–298 (1939).
23. Katsutoshi, T, *Adhesion Theory for Low Friction on Ice*. New Tribological Ways, InTech (2011)
24. Mielonen, K, Jiang, Y, Voyer, J, Diem, A, Hillman, L, Suvanto, M, Pakkanen, TA, ''Sliding Friction of Hierarchically Micro–Micro Textured Polymer Surfaces on Ice.'' *Cold Regions Sci. Technol.*, **163** 8–18 (2019). https://doi.org/10.1016/j.coldregions.2019.04.002
25. D638-14 Standard Test Method for Tensile Properties of Plastics. ASTM International (2014). https://doi.org/10.1520/D0638-14
26. Johnston, ID, McCluskey, DK, Tan, CKL, Tracey, MC, ''Mechanical Characterization of Bulk Sylgard 184 for Microfluidics and Microengineering.'' *J. Micromechan Microeng.*, **24**(3) (2014). https://doi.org/10.1088/0960-1317/24/3/035017
27. Makkonen, L., ''Ice Adhesion—Theory, Measurements and Countermeasures.'' *J Adhes. Sci. Technol.*, **26**(4–5), 413–445. https://doi.org/10.1163/016942411x574583
28. Wang, C, Fuller, T, Zhang, W, Wynne, KJ, ''Thickness Dependence of Ice Removal Stress for a Polydimethylsiloxane Nanocomposite: Sylgard 184.'' *Langmuir*, **30** (43) 12819–12826 (2014). https://doi.org/10.1021/la5030444
29. Nisbet, R, Miner, G, Yale, K, ''Model Evaluation and Enhancement.'' In: *Handbook of Statistical Analysis and Data Mining Applications,* pp. 215–233. (2018)
30. Brewe, DE, Hamrock, BJ, ''Simplified Solution for Elliptical Contact Deformation Between Two Elastic Solids. Transactions ASME.'' *J. Lub. Technol.*, **99** 485–487 (1977)
31. Kreder, MJ, Alvarenga, J, Kim, P, Aizenberg, J, ''Design of Anti-Icing Surfaces: Smooth, Textured or Slippery?'' *Nature Rev. Mater.*, **1**(1) (2016). https://doi.org/10.1038/natrevmats.2015.3
32. Wang, F, Ding, W, He, J, Zhang, Z, ''Phase Transition Enabled Durable Anti-Icing Surfaces and its DIY Design.'' *Chem. Eng. J.*, **360** 243–249 (2019). https://doi.org/10.1016/j.cej.2018.11.224
33. Golovin, K, Kobaku, SP, Lee, DH, DiLoreto, ET, Mabry, JM, Tuteja, A, ''Designing Durable Icephobic Surfaces.'' *Sci. Adv.*, **2**(3) e1501496 (2016). https://doi.org/10.1126/sciadv.1501496